

One-Step Preparation of RGO/Fe₃O₄-FeVO₄ Nanocomposites As Highly Effective Photocatalysts Under Natural Sunlight Illumination

Qana A. Alsulami (✉ qaiselami@kau.edu.sa)

King Abdulaziz University

A. Rajeh

Amran University

Mohammed A. Mannaa

Amran University

Soha M. Albukhari

King Abdulaziz University

Doaa F. Baamer

King Abdulaziz University

Research Article

Keywords: RGO/Fe₃O₄-FeVO₄ nanocomposites, Photocatalysis, Sunlight irradiation, Methylene blue, Phenol, Brilliant green

Posted Date: January 7th, 2022

DOI: <https://doi.org/10.21203/rs.3.rs-1226409/v1>

License:  This work is licensed under a Creative Commons Attribution 4.0 International License.

[Read Full License](#)

Version of Record: A version of this preprint was published at Scientific Reports on April 21st, 2022. See the published version at <https://doi.org/10.1038/s41598-022-10542-z>.

Abstract

The study used a one-step hydrothermal method to prepare $\text{Fe}_3\text{O}_4\text{-FeVO}_4$ and $x\text{RGO}/\text{Fe}_3\text{O}_4\text{-FeVO}_4$ nanocomposites. XRD, TEM, EDS, XPS, DRS, and PL techniques were used to examine the structural and morphological properties of the prepared samples. The XRD results appeared that the $\text{Fe}_3\text{O}_4\text{-FeVO}_4$ has a triclinic crystal structure. Under hydrothermal treatment, (GO) was effectively reduced to (RGO) as illustrated by XRD and XPS results. UV-Vis analysis revealed that the addition of RGO enhanced the absorption in the visible region and narrowed the band gap energy. The photoactivities of the prepared samples were evaluated by degrading methylene blue (MB), phenol and brilliant green (BG) under sunlight illumination. As indicated by all the nanocomposites, photocatalytic activity was higher than the pure $\text{Fe}_3\text{O}_4\text{-FeVO}_4$ photocatalyst, and the highest photodegradation efficiency of MB and phenol was shown by the 10%RGO/ $\text{Fe}_3\text{O}_4\text{-FeVO}_4$. In addition, the study examined the mineralization (TOC), photodegradation process, and photocatalytic reaction kinetics of MB and phenol.

1. Introduction

The world of today is seeking state-of-the-art technologies to deal with the major challenges of the environment pollutions [1–4]. The fast industry expansion and development, water becomes contaminated, carrying significant concentrations of hazardous and dangerous contaminants such as dyes, inks, pesticides, and so on [5–7]. Almost 10 to 15% of dyes are released in the environment during the dying process, contaminating sewage water[8]. Many attempts were taken in order to use new and various light sources and nanomaterials for removal of organic pollutants by photodegradation method [9–11]. Meta-vanadates, which are characterized as cohesive materials' class and have prospective uses in various fields, are one of former mentioned materials[1, 2]. In addition, because of its various stable oxidizing states (+2 to +5), vanadium interacts with numerous components. However, FeVO_4 gave low photocatalytic activity, low optical absorption and poor transport of photogenerated charges which limited its applications [12, 13]. Many novel composites are created as a result of this combining procedure [14]. $\text{Fe}_3\text{O}_4\text{-FeVO}_4$ in particular stands out for its broad range of beneficial properties. It has been investigated for distinctive applications due to its advantageous properties, including ease of preparation, low cost, environmental friendliness, and small band gap [15–17]. The present investigation could not be carried out without $\text{Fe}_3\text{O}_4\text{-FeVO}_4$ feature of small band gap (2.7 to 2.03 eV) [1, 18]. Furthermore, $\text{Fe}_3\text{O}_4\text{-FeVO}_4$ has the necessary conductivity and energy levels to format nanocomposite catalysts [1]. In addition, it was revealed that $\text{Fe}_3\text{O}_4\text{-FeVO}_4$ catalysts were effective applied in the treatment of various organic contaminants present in water over a wider pH range. A varying of methods were applied for water purification [18, 19]. The photocatalysis method does not entail an issue of waste disposal. Furthermore, a lot of composite materials were prepared with graphene and the resultant composites displayed different advantages and applied in various sectors. For example, various composites including $\text{FeVO}_4 \cdot x\text{H}_2\text{O}/\text{Graphene}$ [20], $\text{ZnO}/\text{ZnO}/\text{FeVO}_4$ [21], $\text{FeVO}_4/\text{Bi}_7\text{O}_9\text{I}_3$ [22] rGO- FeVO_4 [23], have recently been prepared and applied in different sectors. In addition, RGO-based ortho-vanadates were applied as useful material for water [3, 19]. In this research, $\text{Fe}_3\text{O}_4\text{-FeVO}_4$ and $x\text{RGO}/\text{Fe}_3\text{O}_4\text{-FeVO}_4$

with various RGO quantities were prepared. The hydrothermal technique was used to efficiently decrease GO to RGO. The study was investigated the influence of RGO quantity on the structural characteristics and photocatalytic effectiveness of $\text{Fe}_3\text{O}_4\text{-FeVO}_4$. The photocatalytic activities of the prepared samples were examined by the photodegradation of MB, phenol and BG solution under natural sunlight illumination. The $\text{xRGO/Fe}_3\text{O}_4\text{-FeVO}_4$ demonstrated excellent charges separation, stability, reusability, and photocatalytic activity, indicating that it is a potential material for a variety of environmental applications.

2. Experimental

2.1. Preparation of GO

Graphene oxide (GO) was prepared as described in our previous literature [24]

2.2. Preparation of $\text{Fe}_3\text{O}_4\text{-FeVO}_4$ and $\text{xRGO/Fe}_3\text{O}_4\text{-FeVO}_4$ nanocomposites

The hydrothermal technique was used to produce $\text{Fe}_3\text{O}_4\text{-FeVO}_4$ and $\text{xRGO/Fe}_3\text{O}_4\text{-FeVO}_4$ nanocomposites. According to this technique, 3 mmol of $\text{Fe}(\text{NO}_3)_3 \cdot 9\text{H}_2\text{O}$ was dissolved in 10 ml of HNO_3 solution with the concentration of 1 mol/L. 3 mmol NH_4VO_3 (Sigma-Aldrich) was dissolved in 10 ml of deionized water and kept at ultrasonic bath @50°C for 30 min. After that, the solution of $\text{Fe}(\text{NO}_3)_3$ was added into NH_4VO_3 solution under vigorous agitation for 1 hour. A certain quantity of the prepared GO was suspended in 20 ml of ethanol solution (2:1) under vigorously stirring and ultrasonicated for 1 hour and then added to the mixture under magnetic agitation for 2 hours. Finally, the resultant mixture was transferred to an autoclave with 50 ml volume and kept at 200°C for 2 h. In comparison, a similar technique was used to produce pure $\text{Fe}_3\text{O}_4\text{-FeVO}_4$ without RGO.

2.3. Characterization methods

Crystal structure of the prepared samples was characterized by X-ray diffraction (XRD, Bruker-D8-AXS diffractometer, Germany) with Cu-K α radiation at a setting of 40 kV and 150 mA. The images were captured using a transmission electron microscope (TEM) with a Jeol JEM-1230 apparatus operating at 120 kV. With the same EDAX detector, an energy-dispersive X-ray (EDx) study was performed (SEM, Hitachi S-4200). The chemical compositions (Axis Ultra DLD, Kratos) were performed using X-ray photoelectron spectroscopy (XPS) with a 325 nm excitation wavelength. At room temperature, UV-Visible absorption studies were conducted by the UV-Vis 2450 (Shimadzu) spectrophotometer to record diffuse reflectance spectra (DRS). The photoluminescence (PL) spectra were carried out with a fluorescent spectrophotometer (HORIBA-Jobin-Yvon).

2.4. Photocatalytic activity study

2.4.1. Photodegradation studies

The photocatalytic activity of the produced catalysts was assessed for MB, phenol and BG photodegradation. Natural sunshine provided irradiation, and the reactor was encased in a water-cooling system. The solution was transported to the photoreactor after 0.05 g of sample powder was added to 50 ml of pollutant ($C_0 = 10$ MB/L). The degradation of MB, phenol and BG in solar light was performed on sunny days between 11 a.m. and 2 p.m. The mixture was first agitated in the dark for 30 minutes to achieve the adsorption-desorption equilibrium. The mixture was then stirred on a magnetically under direct sunshine lighting. The degradation of MB, phenol and BG was calculated using the equation(1) [25], and the change in pollutant concentrations was measured using a UV-vis spectrophotometer.

$$D\% = \left(\frac{C_0 - C_t}{C_0} \right) \times 100\%(1)$$

Where, C_0 and C_t represent the concentrations dyes before and after irradiation, respectively (t). The reactive radicals that might be formed in photocatalytic processes were also investigated employing several scavengers at concentrations of 1 mM, including benzoquinone (BQ), isopropanol (IPA), and Na_2EDTA as $\cdot\text{O}_2^-$, $\cdot\text{OH}$, and h^+ scavengers, respectively [26–28]. The total organic carbon (TOC) was measured using a Shimadzu 5000 TOC Analyzer which applied to investigate the mineralization of MB, phenol and BG. After photodegradation, the %TOC of MB, phenol and BG was estimated using the following equation:

$$\% \text{TOC} = \left(\frac{\text{TOC}_{\text{Initial}} - \text{TOC}_{\text{Final}}}{\text{TOC}_{\text{Initial}}} \right) \times 100(2)$$

3. Results And Discussion

3.1. XRD analysis

The XRD patterns of $\text{Fe}_3\text{O}_4\text{-FeVO}_4$ and $x\text{RGO}/\text{Fe}_3\text{O}_4\text{-FeVO}_4$ nanocomposites are displayed in Fig. 1. The diffraction peaks of $\text{Fe}_3\text{O}_4\text{-FeVO}_4$ demonstrates that the sample have a triclinic phase (JCPDS card No.#71–1592) [29–32]. Further, another diffraction peaks appeared at 18.51° , 30.24° , 35.61° and 73.91° matched very well with the Fe_3O_4 structure (JCPDS No. 19-0629) [33].

The XRD patterns of $x\text{RGO}/\text{Fe}_3\text{O}_4\text{-FeVO}_4$ showed similar peaks as of $\text{Fe}_3\text{O}_4\text{-FeVO}_4$. Moreover, the sample with 15 wt.% of RGO displayed a small peak appeared at $2\theta = 26.05^\circ$ indicating the existence of RGO [20, 34]. As seen in Fig. 1S displays positional shift of the peaks after the addition of RGO. This resulted from effect the introduction of RGO which led to changes in the lattice parameters of $\text{Fe}_3\text{O}_4\text{-FeVO}_4$ (d-spacing changed from 3.17 to 3.19 Å at $2\theta = 27.9^\circ$). In addition, Fig. 1 illustrates that the intensity of characteristic peaks increased with the percentage of RGO increased.

The crystal size of the prepared samples was calculated according to the Scherrer's

equation [35, 36]. Table 1 illustrates that the crystals size of xRGO/Fe₃O₄-FeVO₄ increased with the percentage of RGO increased compared to pure Fe₃O₄-FeVO₄ indicating the existence of RGO enhanced the crystals growth of Fe₃O₄-FeVO₄.

Table 1
Crystallite size and BG energy of the prepared photocatalysts.

Sample name	Crystallite size D (nm)	Band gap energy (eV)
Fe ₃ O ₄ -FeVO ₄	72.9	2.07
5%RGO/ Fe ₃ O ₄ -FeVO ₄	79.6	2.04
10%RGO/ Fe ₃ O ₄ -FeVO ₄	88.1	1.9
15%RGO/ Fe ₃ O ₄ -FeVO ₄	85.8	1.98

3.2. TEM and EDX analysis

The morphology and size of Fe₃O₄-FeVO₄ and xRGO/Fe₃O₄-FeVO₄ were characterized by TEM as depicted in Fig. 2. Fig. 2 (a, b) reveals that the Fe₃O₄-FeVO₄ have nanorod and spherical particles structures. The particles with nanorod structure indicate to the structure of Fe₃O₄-FeVO₄ while the spherical particles attribute to the Fe₃O₄. On the other hand, the particles with nanorods structure showed average size ~138 nm and ~20 nm in length and diameter while the spherical particles is 13.8 nm. Fig. 2 (c) illustrates the influence of the addition of reduced graphene oxide on the structure of Fe₃O₄-FeVO₄. TEM images of 10%Fe₃O₄-FeVO₄ (Fig. 2(c)) displays that the particles still have the nanorods shape. The HR-TEM images of Fe₃O₄-FeVO₄ and 10%RGO/Fe₃O₄-FeVO₄ are shown in Fig. 2(c) and Fig. 2(e) and displays that the d-spacing are 0.30, 0.32 and 0.33 nm where 0.30 nm approach to the (220) lattice plane of Fe₃O₄ (peak at 2 Θ = 30.24°) while 0.32 nm belong to (1-12) plane of FeVO₄ (2 Θ = 27.9°). The increasing in the lattice spacing from 0.30 of Fe₃O₄-FeVO₄ to 0.32 nm of 10%RGO/Fe₃O₄-FeVO₄ resulted from effect the introduction of RGO as described in the XRD. In addition, Fig. 2(e) also reveals the formation of heterojunction interface between FeVO₄ and Fe₃O₄ on the RGO surface.

Figure 3 shows the EDX spectra of Fe₃O₄-FeVO₄ and xRGO/Fe₃O₄-FeVO₄. Fig. 3a displays that the Fe₃O₄-FeVO₄ have Fe, V, C and O and no another impurities were detected. In addition, the 10%RGO/Fe₃O₄-FeVO₄ nanocomposites (Fig. 3b) showed the similar elements as Fe₃O₄-FeVO₄ and C which attributes to RGO in the sample.

3.3. XPS studies

Figure 4 displays the XPS results of Fe₃O₄-FeVO₄ and 10%RGO/Fe₃O₄-FeVO₄. The XPS spectrum of Fe₃O₄-FeVO₄ in Figure 4(a) presents peaks corresponding to Fe 2p, V 2p, and O 1s and the spectrum of

10%RGO/Fe₃O₄-FeVO₄ showed the same peaks as Fe₃O₄-FeVO₄ and C 1S in agreement with EDX results (Fig. 3).

The high-resolution spectra of Fe 2p, V 2p, O1s and C 1s are illustrated in Fig. 4b-d. As seen in Fig. 4b, Fe₃O₄-FeVO₄ displayed main binding energies appeared at 711.23 eV and 725.12 eV belongs to Fe 2p_{3/2} and Fe 2p_{1/2} respectively. Also, the satellite peak appeared at 717.45 eV assigned to Fe³⁺ in the sample [20, 37, 38]. Another peaks observed at 713.33 and 726.86 eV accompanied with its satellite appeared at 720.62 and 733.21 eV which confirmed the presence of Fe²⁺ [20]. Comparing with Fe₃O₄-FeVO₄, 10%RGO/Fe₃O₄-FeVO₄ displayed the same main binding energies as shown in Fig. 4b. Also, the intensity peaks of 10%RGO/Fe₃O₄-FeVO₄ are higher than that of Fe₃O₄-FeVO₄. Fig. 4c shows the high-resolution spectrum of Fe₃O₄-FeVO₄. In this spectrum, six peaks were observed at 516.66, 516.83, 517.22, 523.14, 523.65 and 524.75 eV belong to V 2p_{3/2} and V 2p_{1/2} peaks. The positions of these peaks donating the existence of V⁴⁺ and V⁵⁺ of V [12, 31, 39]. New peaks located at 518.13 eV were observed in the spectrum of 10%RGO/Fe₃O₄-FeVO₄ comparing with Fe₃O₄-FeVO₄. Also, Fig. 4c displays that the peaks located at 516.66 and 523.65 eV were shifted to 516.13 and 521.47 eV, respectively indicating the presence V³⁺ resulted due to the reduction of V⁴⁺ to V³⁺ state [22, 40]. The formation of V⁴⁺ and V³⁺ in the sample indicates to existence of oxygen vacancies (Vo) in their crystal structure [22].

Figure 4d illustrates the spectrum of O1s of Fe₃O₄-FeVO₄ showed three peaks located at 529.92, 530.37 and 532.54 eV assign to the lattice O in Fe₃O₄-FeVO₄ [22, 41]. However, 10%RGO/Fe₃O₄-FeVO₄ exhibited new peaks located at 529.46 and 531.66 eV attributed to the oxygen and hydroxyl groups on the RGO [39, 42, 43]. Also, Figure 4d shows that the binding energies peaks of O 1s in the 10%RGO/Fe₃O₄-FeVO₄ were shifted to 529.97, 530.47 and 532.84 eV, indicating the existence of high Vo formed after the addition of RGO [44]. Fig. 2S gives compression between GO and RGO. In the XPS spectrum of GO (Fig. 2S), four peaks appear at 284.59, 286.28, 288.33 and 289.06 eV are attributed to sp² and sp³ carbon [45–47]. However, positional shift of the peaks located at 288.33 and 289.06 eV to 287.84 and 288.91 eV in the 10%RGO/Fe₃O₄-FeVO₄ were observed and the intensity of peaks that attributed to oxygenated groups were decreased sharply which indicates the effective reduction of GO to RGO [46, 48]. Based on the results above the shifting in the peaks position of Fe 2p, V 2p and O1s in the 10%RGO/Fe₃O₄-FeVO₄ attribute to the strong interactions between Fe₃O₄-FeVO₄ and RGO in the nanocomposites [22, 43].

3.4. DRS analyst

DRS spectra of Fe₃O₄-FeVO₄ and xRGO/Fe₃O₄-FeVO₄ with different RGO contents are depicted in Fig. 5. As depicted in Fig. 5, the samples showed strong absorption in the visible region. The absorbance threshold of Fe₃O₄-FeVO₄ appeared nearly at 705 nm. However, the absorption in the visible region (strong red-shift) improved largely in the xRGO/Fe₃O₄-FeVO₄ comparing with Fe₃O₄-FeVO₄ indicating improving the optical properties Fe₃O₄-FeVO₄ when composed with RGO [49].

The band gap energies (BG) of the prepared samples were calculated and given in Fig. 3S and Table 1. As shown in Table 1, the band gap energy (BG) of $\text{Fe}_3\text{O}_4\text{-FeVO}_4$ is 2.06 eV whereas the BG of $\text{xRGO/Fe}_3\text{O}_4\text{-FeVO}_4$ were narrowed from 2.04 of sample with 5%wt.% of RGO to 1.97 of sample 15wt.% of RGO. The reducing in the BG of $\text{xRGO/Fe}_3\text{O}_4\text{-FeVO}_4$ can attribute to the effect and overlapping of different factors. New orbitals can formed in the $\text{xRGO/Fe}_3\text{O}_4\text{-FeVO}_4$ due to the electronic interactions between RGO and $\text{Fe}_3\text{O}_4\text{-FeVO}_4$ leading narrowing in the BG of $\text{xRGO/Fe}_3\text{O}_4\text{-FeVO}_4$ [42, 50]. Another reason attributes to increasing the V_o in the nanocomposite after the addition of RGO which contributes in the narrowing of BG of $\text{Fe}_3\text{O}_4\text{-FeVO}_4$ due to creation of intermediated states of energy levels in the BG of $\text{xRGO/Fe}_3\text{O}_4\text{-FeVO}_4$ causing narrowing in the BG [51–53].

The creation of intermediated energy states and new molecular orbitals in the $\text{xRGO/Fe}_3\text{O}_4\text{-FeVO}_4$ improved the absorption in the visible region and also contributed in retarding the recombination of photocarriers charges leading improving the photoactivity of $\text{xRGO/Fe}_3\text{O}_4\text{-FeVO}_4$ under solar light [50].

3.5. PL spectra

The photoluminescence spectra (PL) of $\text{Fe}_3\text{O}_4\text{-FeVO}_4$ and $\text{xRGO/Fe}_3\text{O}_4\text{-FeVO}_4$ are displayed in Fig. 6. All samples displayed similar PL spectra and the emission peaks intensities of $\text{xRGO/Fe}_3\text{O}_4\text{-FeVO}_4$ were noticeably decreased compared to the $\text{Fe}_3\text{O}_4\text{-FeVO}_4$, denoting the retardation of charges carriers (e-h) recombination after addition of RGO. On the other hand, Fig. 6 illustrates that the 10%RGO/ $\text{Fe}_3\text{O}_4\text{-FeVO}_4$ displayed the lowest intensity indicating the sample with 10wt.% of RGO effectively separated the photogenerated carriers. The enhancing in the suppression of photocarriers of $\text{xRGO/Fe}_3\text{O}_4\text{-FeVO}_4$ resulted from the role of RGO which acting as an efficiency of electrons trapping by creating of new defects or vacancies within the $\text{Fe}_3\text{O}_4\text{-FeVO}_4$ which in turn enhanced the lifetime of photocarriers [54]. However, increasing the RGO amount beyond 10wt.% led to increasing the PL emission intensity (Fig. 6) indicating the opposite role of RGO where played as recombination centers and consequently accelerated the recombination rate of charges in the $\text{xRGO/Fe}_3\text{O}_4\text{-FeVO}_4$ [25, 46, 50].

3.6. Photocurrent analysis

The transient photocurrent response of the prepared samples was determined under visible light [55]. Fig. 4S exhibits stable and reversible photocurrent densities of the prepared catalysts after several runs of on and off. Also, Fig. 4S displays that the 10%RGO/ $\text{Fe}_3\text{O}_4\text{-FeVO}_4$ showed the highest density comparing to other samples. Based on these results, the photocurrent density of the prepared catalysts strongly depends on the RGO content. These observations confirm the role of RGO in retardation the recombination and improving the transfer of photogenerated charges [56]. However, a reduction in the photocurrent response was observed after increasing the content of RGO to 15 wt.% indicating the opposite role of RGO as described above which in turn reduce the density of photocurrent.

3.7. Photocatalytic performance

3.7.1. Photodegradation studies

The photocatalytic performances of all the prepared samples have been evaluated by the photodegradation of MB, phenol and BG under sunlight irradiation as displayed in Fig. 7 and Fig. 5S, respectively. No photoreaction was observed in absence the catalyst or light source. Comparing with $\text{Fe}_3\text{O}_4\text{-FeVO}_4$, the $\text{xRGO/Fe}_3\text{O}_4\text{-FeVO}_4$ showed the highest photocatalytic activity against of MB, phenol and BG. Also, the sample with 10 wt.% of RGO displayed the highest photoactivity compared with other samples. These results indicate that the addition of RGO enhanced the photocatalytic activity of $\text{Fe}_3\text{O}_4\text{-FeVO}_4$ by enhancing the suppression of the photogenerated charges recombination which in turn improved effectively the photoactivity of $\text{Fe}_3\text{O}_4\text{-FeVO}_4$ under sunlight irradiation [50]

The total effect of RGO in improving and reducing the photoactivity of $\text{Fe}_3\text{O}_4\text{-FeVO}_4$ attributed to the following reasons: the improving resulted due to the effect of RGO in acceleration the transition of electrons to the catalyst surface leading inhibition of the photogeneration charges recombination [46]. Also, the addition of RGO facilitated the transition of electrons from VB to CB due to creation of new levels of energy through the BG of $\text{Fe}_3\text{O}_4\text{-FeVO}_4$ which in turn reduced the required energy for this transfer [57]. On the other hand, the reduction in the photoactivity of $\text{Fe}_3\text{O}_4\text{-FeVO}_4$ in the existence of high amount of RGO resulted from the shielding effect of RGO which restrained the absorption of incident photons to arrival at the active sites on the surface of $\text{Fe}_3\text{O}_4\text{-FeVO}_4$ [46]. Moreover, increasing the amount of RGO acted as recombination centers of electrons and holes pairs [25, 46, 50].

According to the Langmuir-Hinshelwood kinetics model, the photodegradation process of MB, phenol and BG over $\text{Fe}_3\text{O}_4\text{-FeVO}_4$ and $\text{xRGO/Fe}_3\text{O}_4\text{-FeVO}_4$ using the following formula [25]:

$$\ln \left(\frac{C_o}{C_t} \right) = kt$$

where k is the photodegradation rate constant, C_o and C are the original concentration and concentration of pollutant at time t. The linear approximation of the kinetics equation is shown in Fig. 6S. The apparent values of k and correlation coefficient (R^2) were calculated and listed in Table 2. The values of R^2 indicated that the degradation of MB, phenol and BG follows pseudo 1st order kinetics. Also, Table 2 shows the values of k increased with increasing the RGO content and the sample with 10wt.% of RGO displayed the highest photodegradation rate compared with other tested photocatalysts.

Figure 7S illustrates the values of %TOC of MB and phenol degradation over 10%RGO/ $\text{Fe}_3\text{O}_4\text{-FeVO}_4$. The results illustrated that the mineralization of MB and phenol after 180 min was 92.8% and 85.3%, respectively. Comparing these results with the photodegradation results we found the values of %TOC were lower than the photodegradation values. This indicates to existence of some un-degraded intermediates (colorless). However, with increasing the irradiation time to 360 min, the %TOC values increased sharply to achieve 100% of mineralization of both MB and phenol.

Table 1S displays comparison between the photocatalytic activity of our samples that obtained in this work and that found in other literatures [21, 22, 24, 30, 42, 44, 46, 58–62]. As shown in Table 1S the 10%RGO/Fe₃O₄-FeVO₄ showed the highest photoactivity for photodegradation of organic pollutants under solar light. Also, our samples showed high visible light absorption, photogenerated charges separation and reusability. Moreover, in this work, the reduction of graphene oxide was performed effectively without using chemical reduction agents by green reduction method and during short time (2 h) comparing to other literatures.

Table 2
Correlation coefficients and rate constants for MB and phenol photodegradation.

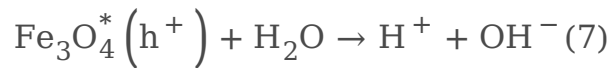
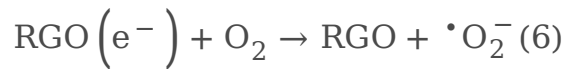
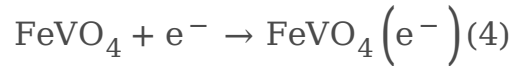
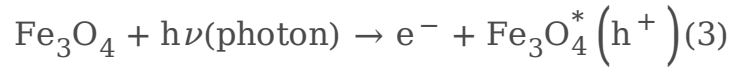
Samples	MB		phenol	
	K ₁	R ²	K ₁	R ²
Fe ₃ O ₄ -FeVO ₄	0.01428	0.99766	0.00592	0.99318
5%RGO/Fe ₃ O ₄ -FeVO ₄	0.02304	0.99862	0.01061	0.99643
10%RGO/Fe ₃ O ₄ -FeVO ₄	0.0601	0.99959	0.02257	0.02257
15%RGO/Fe ₃ O ₄ -FeVO ₄	0.04161	0.9986	0.01599	0.01599

3.7.2. Photocatalytic mechanism

To understand the photodegradation mechanism of MB, the radical scavengers were added during the photodegradation of MB. Fig. 8S shows effect the addition of scavengers on the degradation of MB over 10%RGO/Fe₃O₄-FeVO₄ sample. As shown in Fig. 8S, the addition of BQ ($\cdot\text{O}_2^-$ radical) was accompanied with sharply reduction in the degradation of MB while the addition of Na₂EDTA (h^+ radical) and IPA ($\cdot\text{OH}$ radical) accompanied with high suppression for Na₂EDTA and venial reduction for IPA. These results imply that the $\cdot\text{O}_2^-$ played the main role in degradation of MB while the $\cdot\text{OH}$ played the minor role. This indicates that the $\cdot\text{O}_2^-$ is the more active radical contributed in the degradation of MB.

From the radical scavengers results, the possible mechanism of the degradation of MB, phenol and BG over xRGO/Fe₃O₄-FeVO₄ was suggested as a direct Z-scheme as proposed in Scheme 1. In this mechanism, when the xRGO/Fe₃O₄-FeVO₄ absorbed the sunlight illumination, the incident photons promoted transfer of electrons (e^-) to the CB of FeVO₄ and the holes (h^+) accumulated in the VB of Fe₃O₄ (Eq. (3) & (4)). The photoinduced e^- on the CB of Fe₃O₄ can transfer to the VB of FeVO₄, and then quickly recombine with the h^+ of FeVO₄ were achieved, which is favorable for higher separation rate of e^- - h^+ pairs of the single photocatalyst and higher redox potential [63, 64]. In this case, the e^- accumulated in CB of

FeVO₄ are taken by the RGO and then reduce O₂ into •O₂⁻ (Eq. (5)&(6)), while the h⁺ in VB of Fe₃O₄ VB are more positive potential and has sufficient oxidation capacity to oxidize OH⁻ into •OH or react with pollutants molecules directly (Eq. (7-9)) [63–67]. These results imply the contribution of generated radicals in the degradation of MB and phenol to gives CO₂ and H₂O.



3.7.3. Reusability study

The reusability and stability of 10%RGO/Fe₃O₄-FeVO₄ were studied. Fig. 9S displays the degradation of MB and phenol after four cycles (runs) under the same conditions. The catalyst powder was separated from the reaction mixture after each run and soaked in ethanol for 1 h. Then, the powder was washed with water and finally dried at 100°C for 8 h [27]. The obtain results illustrated no significant decline in photodegradation activity of 10%RGO/Fe₃O₄-FeVO₄ was observed after five runs. To investigate the effect of reused times on the structural properties of catalyst, the 10%RGO/Fe₃O₄-FeVO₄ was investigated by the XRD and TEM techniques before and after reuse as shown in **Fig. 8** and the results showed no changes were observed in the structural properties of 10%RGO/Fe₃O₄-FeVO₄ indicating the excellent reusability and sustainability of the prepared photocatalysts.

4. Conclusion

Fe₃O₄-FeVO₄ and xRGO/Fe₃O₄-FeVO₄ were successfully prepared by the hydrothermal method. The results confirmed successfully reduction GO to RGO by green method. The UV-Vis results showed improving of the absorption in the visible region and enhancing of the photogenerated charges separation of after the addition of RGO. The samples showed excellent degradation of MB, phenol, BG after the addition of RGO under sunlight illumination and the sample with 10 wt.% of RGO exhibited the

highest photodegradation efficiency. The TOC analysis illustrated that the MB and phenol completely mineralized after 360 min. The results of scavenger tests showed that the $\cdot\text{O}_2^-$ played the main role in oxidant of MB. The kinetic studies results illustrated that the degradation of MB and phenol follows the pseudo 1st order kinetics. The prepared samples showed excellent reusability after five runs without significant reduction in the photoactivity. Based on these results, we can be concluded that the xRGO/Fe₃O₄-FeVO₄ are suitable and convenient material for treatment of organic pollutants and industrial effluent.

Declarations

Acknowledgments:

“The authors extend their appreciation to the Deputyship for Research & Innovation, Ministry of Education in Saudi Arabia for funding this research work through the project number IFPHI-027-247-2020.” and King Abdulaziz University, DSR, Jeddah, Saudi Arabia.

References

1. S.K. Biswas, J.O. Baeg, Enhanced photoactivity of visible light responsive W incorporated FeVO₄ photoanode for solar water splitting, *Int. J. Hydrogen Energy*. 38 (2013) 14451–14457.
2. A. Mishra, G. Bera, P. Mal, G. Padmaja, P. Sen, P. Das, B. Chakraborty, G.R. Turpu, Comparative electrochemical analysis of rGO-FeVO₄ nanocomposite and FeVO₄ for supercapacitor application, *Appl. Surf. Sci.* 488 (2019) 221–227.
3. B. Jansi Rani, G. Ravi, R. Yuvakkumar, P. Kumar, S.I. Hong, D. Velauthapillai, M. Thambidurai, C. Dang, Ni supported anorthic phase FeVO₄ nanorods for electrochemical water oxidation, *Mater. Lett.* 275 (2020) 128091.
4. X. Long, L. Gao, F. Li, Y. Hu, S. Wei, C. Wang, T. Wang, J. Jin, J. Ma, Bamboo shoots shaped FeVO₄ passivated ZnO nanorods photoanode for improved charge separation/transfer process towards efficient solar water splitting, *Appl. Catal. B Environ.* 257 (2019) 117813.
5. B. Appavu, S. Thiripuranthagan, S. Ranganathan, E. Erusappan, K. Kannan, BiVO₄/N-rGO nano composites as highly efficient visible active photocatalyst for the degradation of dyes and antibiotics in eco system, in: *Ecotoxicol. Environ. Saf.*, 151 (2018) 118.
6. S.M. Hassan, M.A. Mannaa, Photocatalytic Degradation of Brilliant Green Dye by SnO₂/TiO₂ Nanocatalysts, *Int. J. Nano Mater. Sci.* 5 (2016) 9–19.
7. M. A. Mannaa, H.M. Altass, R.S. Salama, MCM-41 grafted with citric acid: The role of carboxylic groups in enhancing the synthesis of xanthenes and removal of heavy metal ions, *Environ. Nanotechnology, Monit. Manag.* 15 (2021) 100410.
8. M.M. Sajid, N.A. Shad, Y. Javed, S.B. Khan, Z. Zhang, N. Amin, H. Zhai, Morphological effects on the photocatalytic performance of FeVO₄ nanocomposite, *Nano-Structures and Nano-Objects*. 22 (2020)

100431.

9. M.A. Mannaa, K.F. Qasim, F.T. Alshori, S.M. El-bahy, R.S. Salama, Role of NiO Nanoparticles in Enhancing Structure Properties of TiO₂ and Its Applications in Photodegradation and Hydrogen Evolution, 6 (2021) 30386–30400. doi:10.1021/acsomega.1c03693.
10. F.T. Alshori, A.A. Alswat, M.A. Mannaa, M.T. Alotaibi, S.M. El-bahy, R.S. Salama, Facile and Green Synthesis of Silver Quantum Dots Immobilized onto a Polymeric CTS – PEO Blend for the Photocatalytic Degradation of p – Nitrophenol, (2021). doi:10.1021/acsomega.1c03735.
11. H. M. Altass, M. Morad, A. S. Khder, M. A. Mannaa, R.S. Jassas, A.A. Alsimaree, S.A. Ahmed, R.S. Salama, Enhanced Catalytic Activity for CO Oxidation by Highly Active Pd Nanoparticles Supported on Reduced Graphene Oxide/Copper Metal Organic Framework, J. Taiwan Inst. Chem. Eng. 000 (2021) 1–15.
12. M. Zhang, Y. Ma, D. Friedrich, R. Van De Krol, L.H. Wong, F.F. Abdi, Elucidation of the opto-electronic and photoelectrochemical properties of FeVO₄ photoanodes for solar water oxidation, J. Mater. Chem. A. 6 (2018) 548–555.
13. M.M. Sajid, N.A. Shad, Y. Javed, S.B. Khan, Z. Zhang, N. Amin, H. Zhai, Morphological effects on the photocatalytic performance of FeVO₄ nanocomposite, Nano-Structures and Nano-Objects. 22 (2020) 100431.
14. N. Li, X. Wu, M. Wang, K. Huang, J. He, W. Ma, H. Chen, Y. Li, S. Feng, Facile preparation of BiVO₄/FeVO₄ heterostructure for efficient water-splitting applications, Int. J. Hydrogen Energy. 44 (2019) 23046–23053.
15. B. Ozturk, G.S. Pozan Soylu, Synthesis of surfactant-assisted FeVO₄ nanostructure: Characterization and photocatalytic degradation of phenol, J. Mol. Catal. A Chem. 398 (2015) 65–71.
16. A. Chachvalvutikul, J. Jakmunee, S. Thongtem, S. Kittiwachana, S. Kaowphong, Novel FeVO₄/Bi₇O₉I₃ nanocomposite with enhanced photocatalytic dye degradation and photoelectrochemical properties, Appl. Surf. Sci. 475 (2019) 175–184.
17. M.M. Sajid, N.A. Shad, Y. Javed, S.B. Khan, Z. Imran, S. Hassan, Z. Hussain, Z. Zhang, N. Amin, Fast Surface Charge Transfer with Reduced Band Gap Energy of FeVO₄/Graphene Nanocomposite and Study of Its Electrochemical Property and Enhanced Photocatalytic, Arab. J. Sci. Eng., (2019) 44:6659–6667.
18. D.P. Dutta, M. Ramakrishnan, M. Roy, A. Kumar, Effect of transition metal doping on the photocatalytic properties of FeVO₄ nanoparticles, J. Photochem. Photobiol. A Chem. 335 (2017) 102–111.
19. R. Yang, Z. Zhu, C. Hu, S. Zhong, L. Zhang, B. Liu, W. Wang, One-step preparation (3D/2D/2D) BiVO₄/FeVO₄@rGO heterojunction composite photocatalyst for the removal of tetracycline and hexavalent chromium ions in water, Chem. Eng. J., 390 (2020) 944–95.
20. H. Zhang, K. Ye, K. Zhu, R. Cang, J. Yan, K. Cheng, G. Wang, D. Cao, The FeVO₄·0.9H₂O/Graphene composite as anode in aqueous magnesium ion battery, Electrochim. Acta. 256 (2017) 357–364.

21. R. Rahimpour, N. Chaibakhsh, M.A. Zanjanchi, Z. Moradi-Shoeili, Fabrication of ZnO/FeVO₄ heterojunction nanocomposite with high catalytic activity in photo-Fenton-like process, *J. Alloys Compd.* 817 (2020) 152702.
22. A. Chachvalvutikul, J. Jakmunee, S. Thongtem, S. Kittiwachana, S. Kaowphong, Novel FeVO₄/Bi₇O₉I₃ nanocomposite with enhanced photocatalytic dye degradation and photoelectrochemical properties, *Appl. Surf. Sci.* 475 (2019) 175–184.
23. A. Mishra, G. Bera, P. Mal, G. Padmaja, P. Sen, P. Das, B. Chakraborty, G.R. Turpu, Comparative electrochemical analysis of rGO-FeVO₄ nanocomposite and FeVO₄ for supercapacitor application, *Appl. Surf. Sci.* 488 (2019) 221–227.
24. Q.A. Alsulami, A. Rajeh, M.A. Mannaa, S.M. Albukhari, D.F. Baamer, Preparation of highly efficient sunlight driven photodegradation of some organic pollutants and H₂ evolution over rGO/FeVO₄ nanocomposites, *Int. J. Hydrogen Energy.* 46 (2021) 27349–27363.
25. S.M. Hassan, A.I. Ahmed, M.A. Mannaa, Structural, photocatalytic, biological and catalytic properties of SnO₂/TiO₂ nanoparticles, *Ceram. Int.* 44 (2018) 6201–6211.
26. S.M. Hassan, A.I. Ahmed, M.A. Mannaa, Preparation and characterization of SnO₂ doped TiO₂ nanoparticles: Effect of phase changes on the photocatalytic and catalytic activity, *J. Sci. Adv. Mater. Devices.* 4 (2019) 400–412.
27. S.M. Hassan, A.I. Ahmed, M.A. Mannaa, Surface acidity, catalytic and photocatalytic activities of new type H₃PW₁₂O₄₀/Sn-TiO₂ nanoparticles, *Colloids Surfaces A Physicochem. Eng. Asp.* 577 (2019) 147–157.
28. M. Khan, A. Hayat, S.K. Baburao Mane, T. Li, N. Shaishta, D. Alei, T.K. Zhao, A. Ullah, A. Zada, A.U. Rehman, W.U. Khan, Functionalized nano diamond composites for photocatalytic hydrogen evolution and effective pollutant degradation, *Int. J. Hydrogen Energy.* 45 (2020) 29070–29081.
29. B. Jansi Rani, G. Ravi, R. Yuvakkumar, P. Kumar, S.I. Hong, D. Velauthapillai, M. Thambidurai, C. Dang, Ni supported anorthic phase FeVO₄ nanorods for electrochemical water oxidation, *Mater. Lett.* 275 (2020) 128091.
30. D.P. Dutta, M. Ramakrishnan, M. Roy, A. Kumar, Effect of transition metal doping on the photocatalytic properties of FeVO₄ nanoparticles, *J. Photochem. Photobiol. A Chem.* 335 (2017) 102–111.
31. J. Zhang, W. Zhao, Z. Li, G. Lu, M. Zhu, Visible-light-assisted peroxymonosulfate activation over Fe(II)/V(IV) self-doped FeVO₄ nanobelts with enhanced sulfamethoxazole degradation: Performance and mechanism, *Chem. Eng. J.* 403 (2021) 126384.
32. J. Li, W. Zhao, Y. Guo, Z. Wei, M. Han, H. He, S. Yang, C. Sun, Facile synthesis and high activity of novel BiVO₄/FeVO₄ heterojunction photocatalyst for degradation of metronidazole, *Appl. Surf. Sci.* 351 (2015) 270–279.
33. S. Zolfagharinia, E. Kolvari, N. Koukabi, M.M. Hosseini, Core-shell zirconia-coated magnetic nanoparticles offering a strong option to prepare a novel and magnetized heteropolyacid based

- heterogeneous nanocatalyst for three- and four-component reactions, *Arab. J. Chem.* 13 (2020) 227–241.
34. H. Hashtroudi, R. Kumar, R. Savu, S. Moshkalev, G. Kawamura, A. Matsuda, M. Shafiei, Hydrogen gas sensing properties of microwave-assisted 2D Hybrid Pd/rGO: Effect of temperature, humidity and UV illumination, *Int. J. Hydrogen Energy.* 46 (2021) 7653–7665.
 35. S.M.H. Hassan, M.A. Mannaa, A.A. Ibrahim, Nano-sized mesoporous phosphated tin oxide as an efficient solid acid catalyst, *RSC Adv.* 9 (2019) 810–818.
 36. A.A. Ibrahim, S.M. Hassan, M.A. Mannaa, Mesoporous tin oxide-supported phosphomolybdic acid as high performance acid catalysts for the synthesis of hydroquinone diacetate, *Colloids Surfaces A Physicochem. Eng. Asp.* 586 (2020) 124248.
 37. L. Meng, R. Guo, X. Sun, F. Li, J. Peng, C. Chen, T. Li, J. Deng, Enhanced electrochemical performance of a promising anode material FeVO_4 by tungsten doping, *Ceram. Int.* 46 (2020) 21360–21366.
 38. S.K. Biswas, J.O. Baeg, Enhanced photoactivity of visible light responsive W incorporated FeVO_4 photoanode for solar water splitting, *Int. J. Hydrogen Energy.* 38 (2013) 14451–14457.
 39. X. Niu, Y. Zhang, L. Tan, Z. Yang, J. Yang, T. Liu, L. Zeng, Y. Zhu, L. Guo, Amorphous FeVO_4 as a promising anode material for potassium-ion batteries, *Energy Storage Mater.* 22 (2019) 160–167.
 40. B. Lan, C. Tang, L. Chen, W. Zhang, W. Tang, C. Zuo, X. Fu, S. Dong, Q. An, P. Luo, $\text{FeVO}_4 \cdot n\text{H}_2\text{O}@\text{rGO}$ nanocomposite as high performance cathode materials for aqueous Zn-ion batteries, *J. Alloys Compd.* 818 (2020) 153372.
 41. Y. Yu, P. Ju, D. Zhang, X. Han, X. Yin, L. Zheng, C. Sun, Peroxidase-like activity of FeVO_4 nanobelts and its analytical application for optical detection of hydrogen peroxide, *Sensors Actuators, B Chem.* 233 (2016) 162–172.
 42. M.M.J. Sadiq, U.S. Shenoy, D.K. Bhat, Enhanced photocatalytic performance of N-doped RGO- $\text{FeWO}_4/\text{Fe}_3\text{O}_4$ ternary nanocomposite in environmental applications, *Mater. Today Chem.* 4 (2017) 133–141.
 43. X. Long, L. Gao, F. Li, Y. Hu, S. Wei, C. Wang, T. Wang, J. Jin, J. Ma, Bamboo shoots shaped FeVO_4 passivated ZnO nanorods photoanode for improved charge separation/transfer process towards efficient solar water splitting, *Appl. Catal. B Environ.* 257 (2019) 117813.
 44. N. Li, X. Wu, M. Wang, K. Huang, J. He, W. Ma, H. Chen, Y. Li, S. Feng, Facile preparation of $\text{BiVO}_4/\text{FeVO}_4$ heterostructure for efficient water-splitting applications, *Int. J. Hydrogen Energy.* 44 (2019) 23046–23053.
 45. T. Wang, C. Li, J. Ji, Y. Wei, P. Zhang, S. Wang, X. Fan, J. Gong, Reduced graphene oxide (rGO)/ BiVO_4 composites with maximized interfacial coupling for visible light photocatalysis, *ACS Sustain. Chem. Eng.* 2 (2014) 2253–2258.
 46. R. Yang, Z. Zhu, C. Hu, S. Zhong, L. Zhang, B. Liu, W. Wang, One-step preparation (3D/2D/2D) $\text{BiVO}_4/\text{FeVO}_4@\text{rGO}$ heterojunction composite photocatalyst for the removal of tetracycline and hexavalent chromium ions in water, in: *Chem. Eng. J., Elsevier*, 2020: pp. 944–950.

47. Z. Yang, R. He, H. Wu, Y. Ding, H. Mei, Needle-like CoP/rGO growth on nickel foam as an efficient electrocatalyst for hydrogen evolution reaction, *Int. J. Hydrogen Energy*. 46 (2021) 9690–9698.
48. L. Zhang, A. Wang, N. Zhu, B. Sun, Y. Liang, W. Wu, Synthesis of butterfly-like BiVO₄/RGO nanocomposites and their photocatalytic activities, *Chinese J. Chem. Eng.* 26 (2018) 667–674.
49. G.L. He, M.J. Chen, Y.Q. Liu, X. Li, Y.J. Liu, Y.H. Xu, Hydrothermal synthesis of FeWO₄-graphene composites and their photocatalytic activities under visible light, *Appl. Surf. Sci.* 351 (2015) 474–479.
50. D. Fang, X. Li, H. Liu, W. Xu, M. Jiang, W. Li, X. Fan, BiVO₄-rGO with a novel structure on steel fabric used as high-performance photocatalysts, *Sci. Rep.* 7 (2017) 1–9.
51. G. Eshaq, S. Wang, H. Sun, M. Sillanpaa, Superior performance of FeVO₄@CeO₂ uniform core-shell nanostructures in heterogeneous Fenton-sonophotocatalytic degradation of 4-nitrophenol, *J. Hazard. Mater.* 382 (2020) 121059.
52. R. Vinoth, P. Karthik, C. Muthamizhchelvan, B. Neppolian, M. Ashokkumar, Carrier separation and charge transport characteristics of reduced graphene oxide supported visible-light active photocatalysts, *Phys. Chem. Chem. Phys.* 18 (2016) 5179–5191.
53. X. Ren, J. Yao, L. Cai, J. Li, X. Cao, Y. Zhang, B. Wang, Y. Wei, Band gap engineering of BiOI: Via oxygen vacancies induced by graphene for improved photocatalysis, *New J. Chem.* 43 (2019) 1523–1530.
54. M.M. Sajid, N.A. Shad, Y. Javed, S.B. Khan, Z. Imran, S. Hassan, Z. Hussain, Z. Zhang, N. Amin, Fast Surface Charge Transfer with Reduced Band Gap Energy of FeVO₄/Graphene Nanocomposite and Study of Its Electrochemical Property and Enhanced Photocatalytic Activity, *Arab. J. Sci. Eng.* 44 (2019) 6659–6667.
55. W. Peng, S.S. Zhang, Y.B. Shao, J.H. Huang, Bimetallic PtNi/g-C₃N₄ nanotubes with enhanced photocatalytic activity for H₂ evolution under visible light irradiation, *Int. J. Hydrogen Energy*. 43 (2018) 22215–22225.
56. K.L. Chen, S.S. Zhang, J.Q. Yan, W. Peng, D.P. Lei, J.H. Huang, Excellent visible light photocatalytic efficiency of Na and S co-doped g-C₃N₄ nanotubes for H₂ production and organic pollutant degradation, *Int. J. Hydrogen Energy*. 44 (2019) 31916–31929.
57. A. Bashir, F. Bashir, M. Sultan, M. Mubeen, A. Iqbal, Z. Akhter, Influence of nickel and lanthanum ions co-doping on photocatalytic properties of TiO₂ for effective degradation of reactive yellow 145 in the visible region, *J. Sol-Gel Sci. Technol.* 93 (2020) 438–451.
58. H. Chen, J. Zeng, M. Chen, Z. Chen, M. Ji, J. Zhao, J. Xia, H. Li, Improved visible light photocatalytic activity of mesoporous FeVO₄ nanorods synthesized using a reactable ionic liquid, *Cuihua Xuebao/Chinese J. Catal.* 40 (2019) 744–754.
59. X. Liu, Y. Kang, Synthesis and high visible-light activity of novel Bi₂O₃/FeVO₄ heterojunction photocatalyst, *Mater. Lett.* 164 (2016) 229–231.

60. G. Bera, A. Mishra, P. Mal, P. Das, G. Padmaja, P. Rambabu, G.R. Turpu, Methylene blue dye degradation by bulk, nano FeVO_4 and rGO-FeVO_4 , *3Rd Int. Conf. Condens. Matter Appl. Phys.* 2220 (2020) 080070.
61. M.J.S. Mohamed, S. Shenoy U, D.K. Bhat, Novel $\text{NRGO-CoWO}_4\text{-Fe}_2\text{O}_3$ nanocomposite as an efficient catalyst for dye degradation and reduction of 4-nitrophenol, *Mater. Chem. Phys.* 208 (2018) 112–122.
62. B. Appavu, S. Thiripuranthagan, S. Ranganathan, E. Erusappan, K. Kannan, $\text{BiVO}_4/\text{N-rGO}$ nano composites as highly efficient visible active photocatalyst for the degradation of dyes and antibiotics in eco system, in: *Ecotoxicol. Environ. Saf.*, Elsevier Inc., 151 (2018) 118–126.
63. Q. Wang, Z. Liu, Q. Lu, E. Guo, M. Wei, Fabrication of Direct Z-scheme $\alpha\text{-Fe}_2\text{O}_3/\text{FeVO}_4$ Nanobelts with Enhanced Photoelectrochemical Performance, *ChemistrySelect.* 3 (2018) 809–815.
64. G. Xu, M. Du, T. Li, Y. Guan, C. Guo, Facile synthesis of magnetically retrievable $\text{Fe}_3\text{O}_4/\text{BiVO}_4/\text{CdS}$ heterojunction composite for enhanced photocatalytic degradation of tetracycline under visible light, *Sep. Purif. Technol.* 275 (2021) 119157.
65. S. Dehghan, A.J. Jafari, M. FarzadKia, A. Esrafil, R.R. Kalantary, Visible-light-driven photocatalytic degradation of Metalaxyl by reduced graphene oxide/ $\text{Fe}_3\text{O}_4/\text{ZnO}$ ternary nanohybrid: Influential factors, mechanism and toxicity bioassay, *J. Photochem. Photobiol. A Chem.* 375 (2019) 280–292.
66. X. Yan, K. Liu, W. Shi, Facile synthesis of CdS/MnWO_4 heterojunction with enhanced visible-light-driven photocatalytic activity and mechanism investigation, *Colloids Surfaces A Physicochem. Eng. Asp.* 520 (2017) 138–145.
67. T. Xie, H. Li, C. Liu, J. Yang, T. Xiao, L. Xu, Magnetic photocatalyst $\text{BiVO}_4/\text{Mn-Zn}$ ferrite/reduced graphene oxide: Synthesis strategy and its highly photocatalytic activity, *Nanomaterials*, 8 (2018) 944–950.

Figures

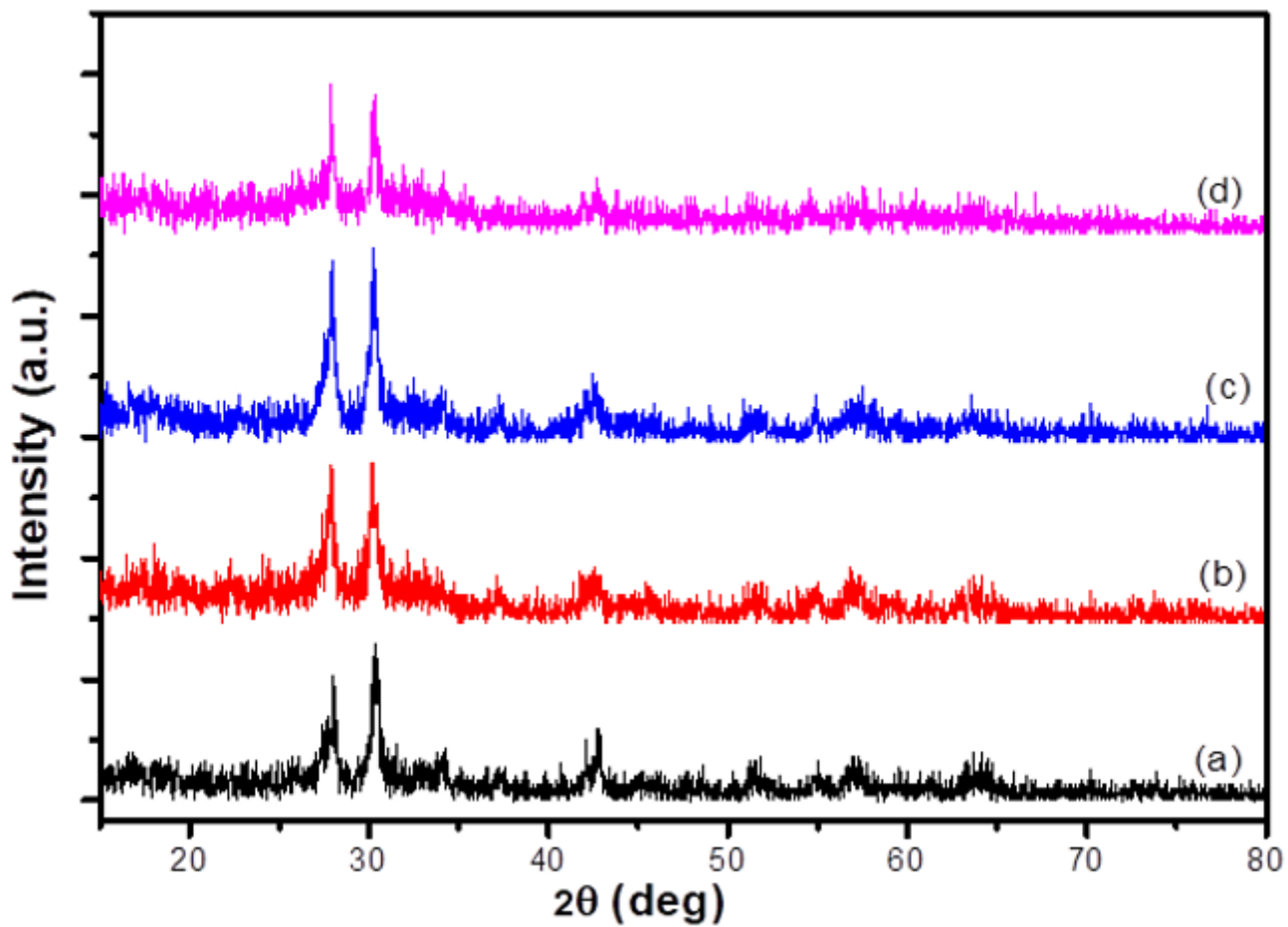


Figure 1

XRD patterns of (a) $\text{Fe}_3\text{O}_4\text{-FeVO}_4$ and (b) 5%, (c) 10%, (d) 15%RGO/ $\text{Fe}_3\text{O}_4\text{-FeVO}_4$ nanocomposites

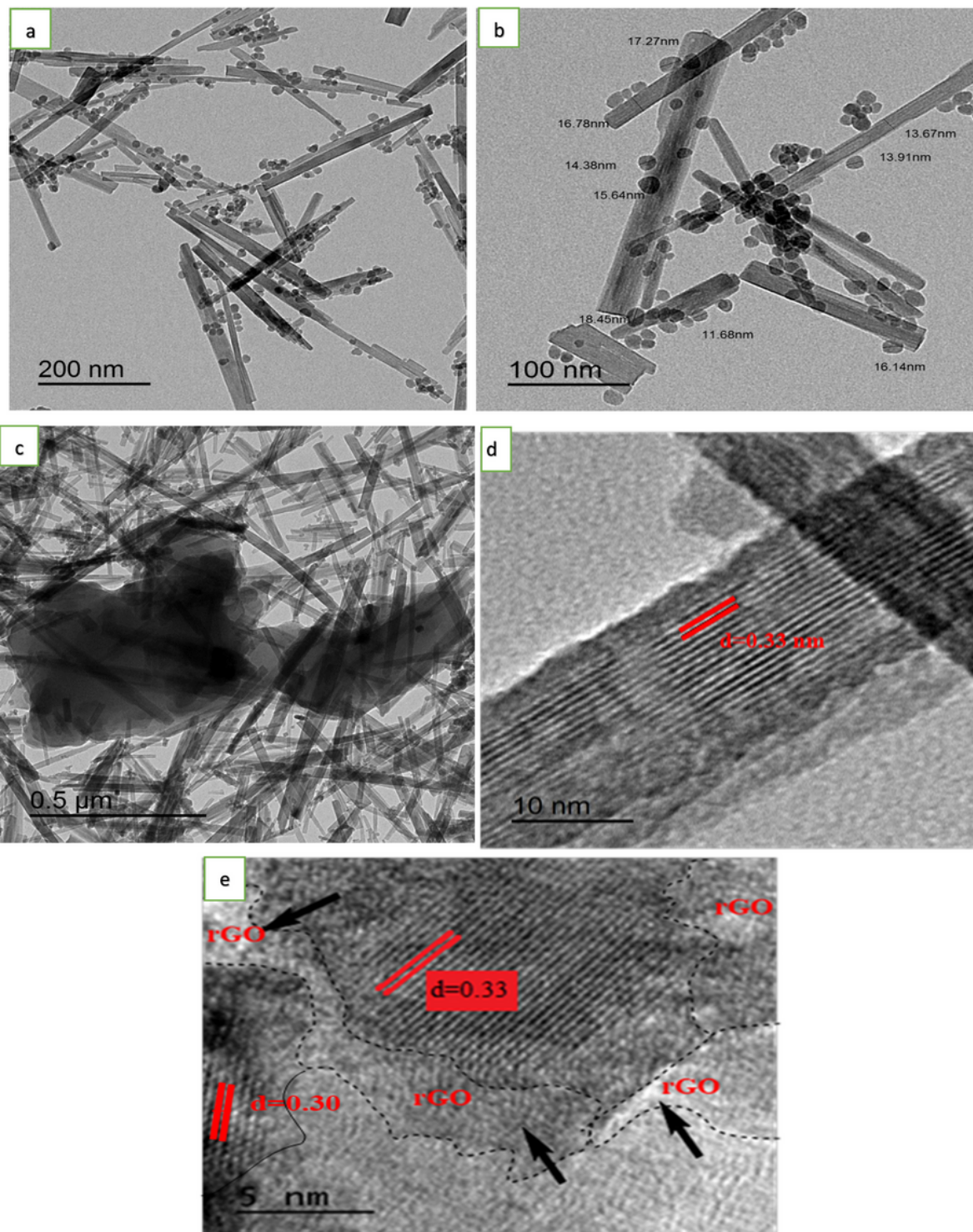


Figure 2

TEM and HR-TEM images of (a, b, d) Fe₃O₄-FeVO₄ and (c, e) 10%RGO/Fe₃O₄-FeVO₄.

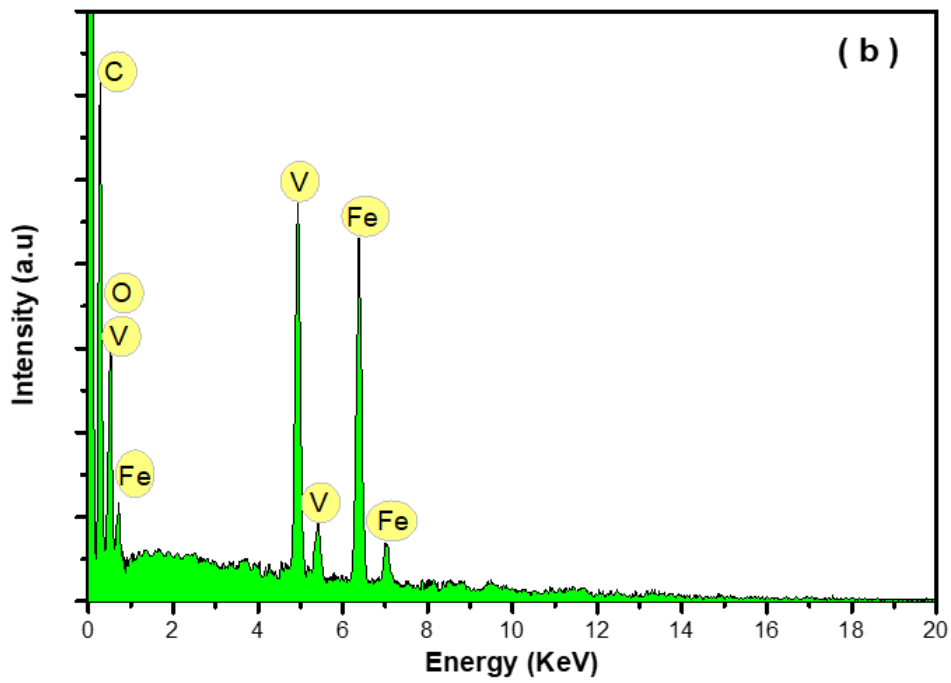
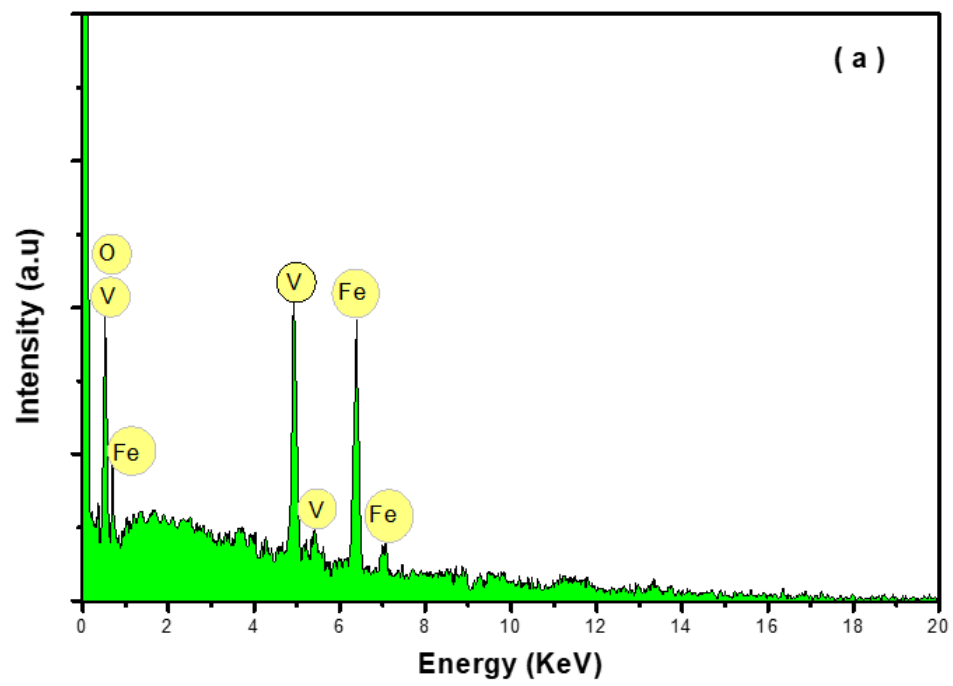


Figure 3

EDX spectra of (a) $\text{Fe}_3\text{O}_4\text{-FeVO}_4$ and (b) 10%RGO/ $\text{Fe}_3\text{O}_4\text{-FeVO}_4$ nanocomposite.

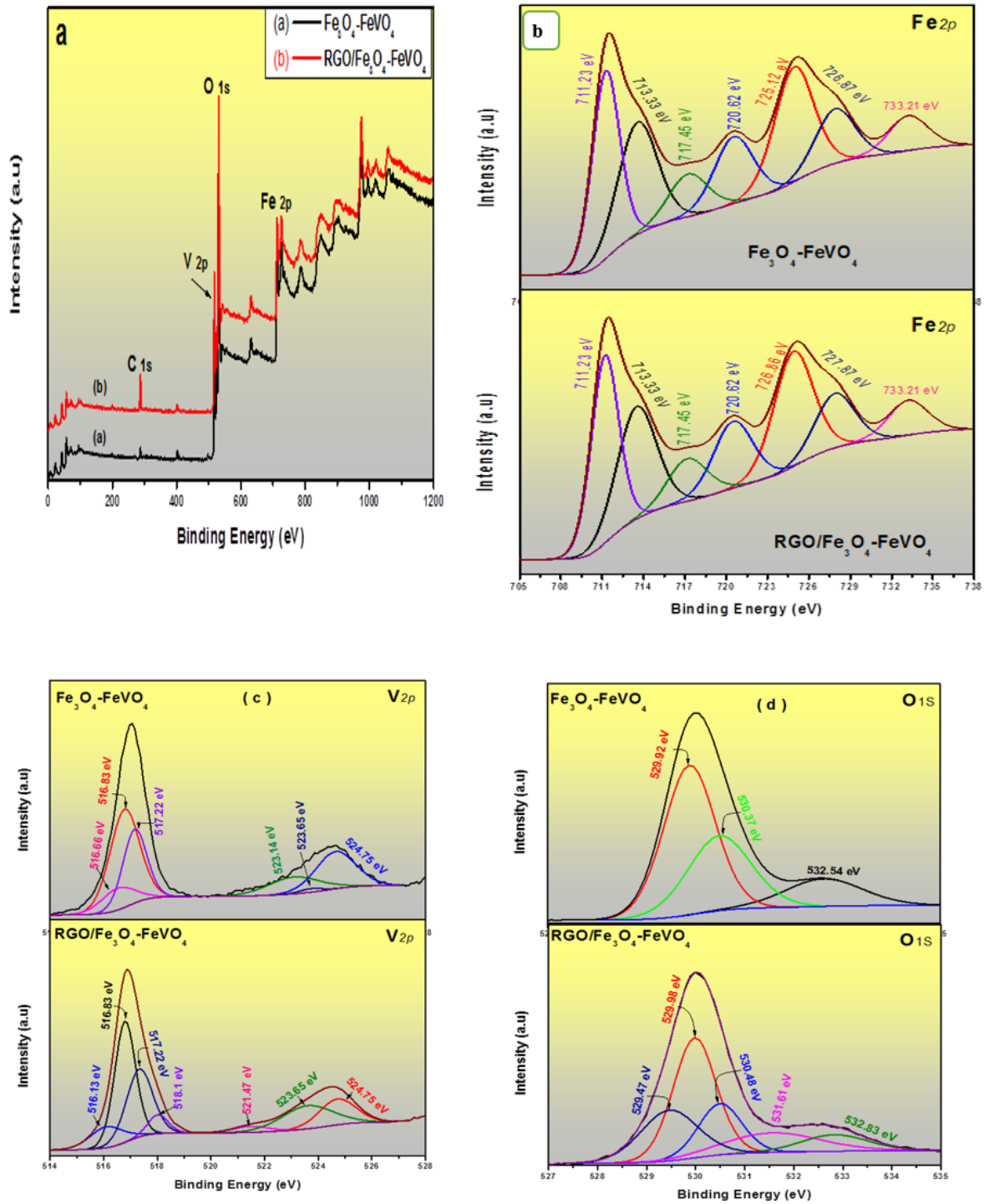


Figure 4

XPS spectra of $\text{Fe}_3\text{O}_4\text{-FeVO}_4$ and 10% $\text{RGO/Fe}_3\text{O}_4\text{-FeVO}_4$ nanocomposites.

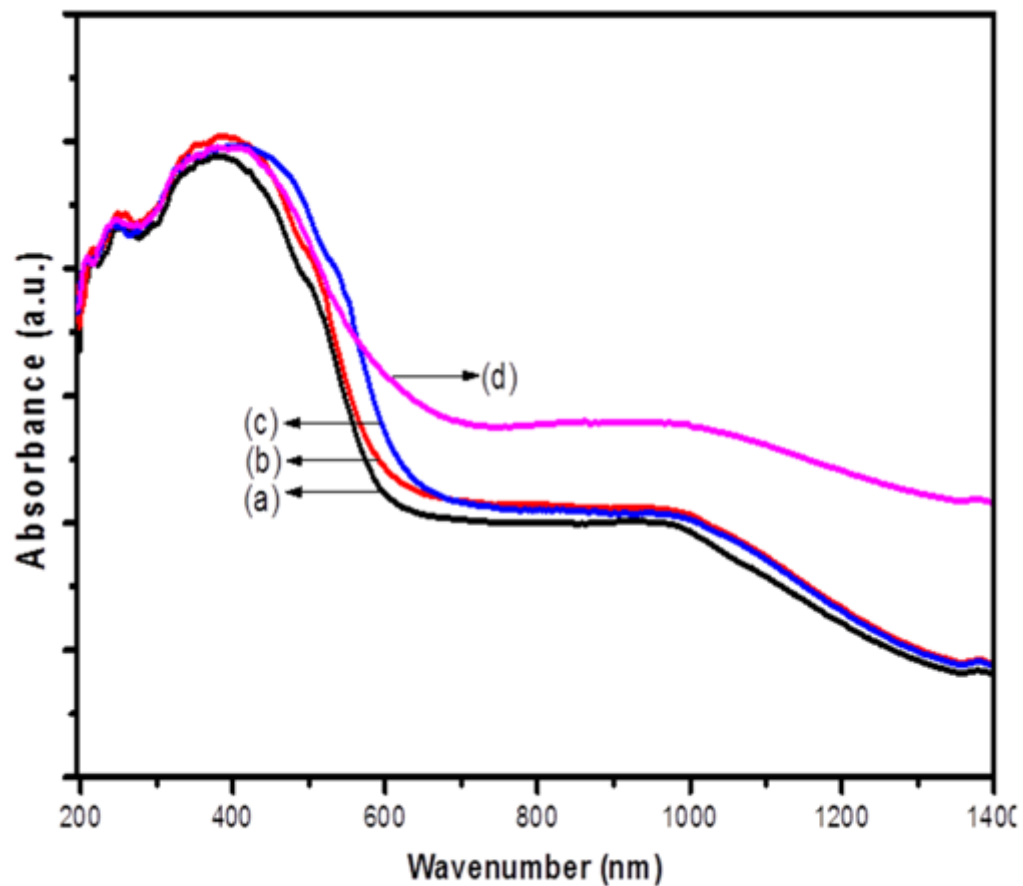


Figure 5

UV-vis absorbance spectra of (a) $\text{Fe}_3\text{O}_4\text{-FeVO}_4$ and $x\text{RGO/Fe}_3\text{O}_4\text{-FeVO}_4$ at (b) 5%, (c) 10%, (d) 15% wt.% of RGO.

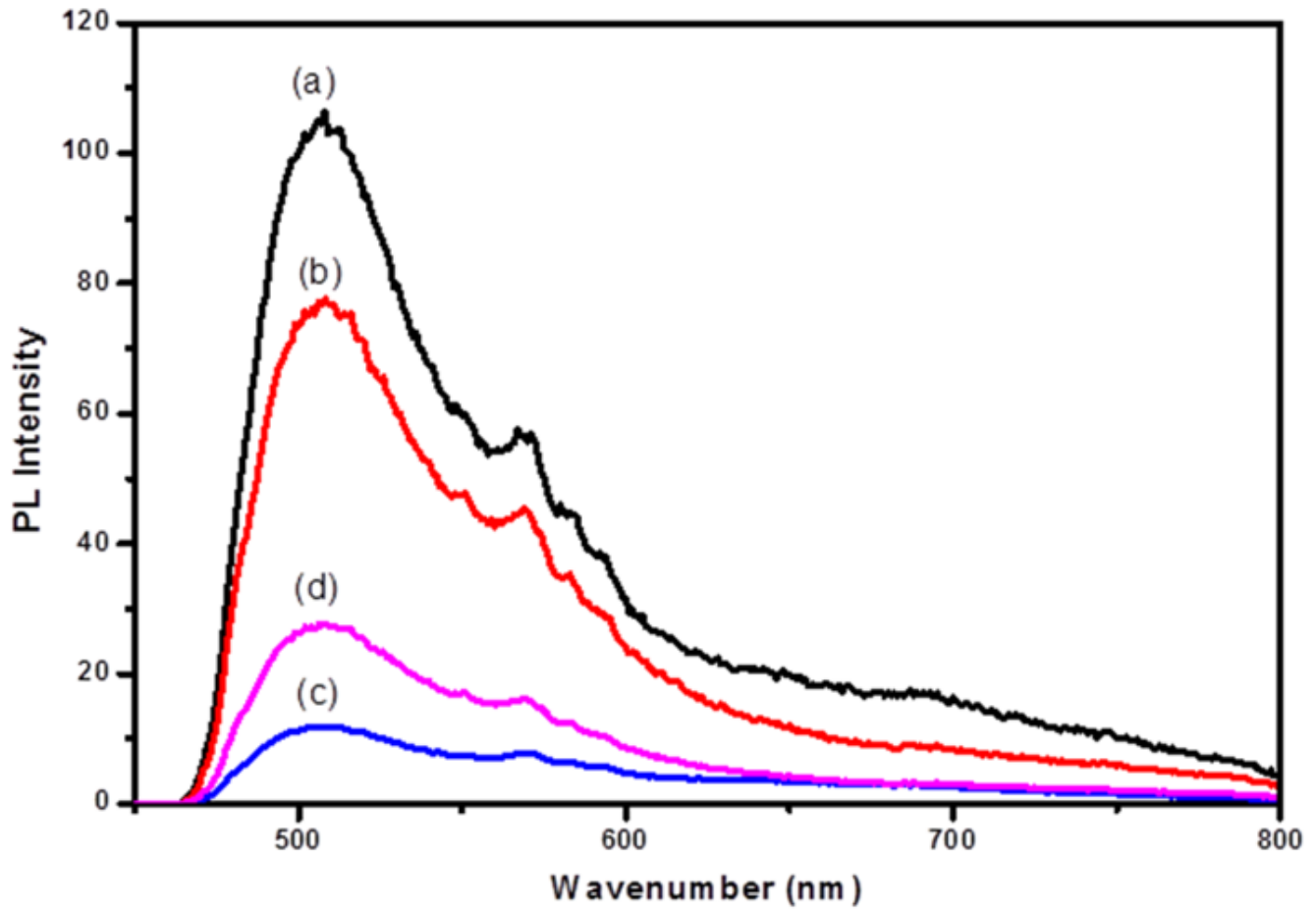


Figure 6

PL spectra of (a) Fe₃O₄-FeVO₄ and xRGO/Fe₃O₄-FeVO₄ at (b) 5%, (c) 10%, (d) 15% wt.% of RGO.

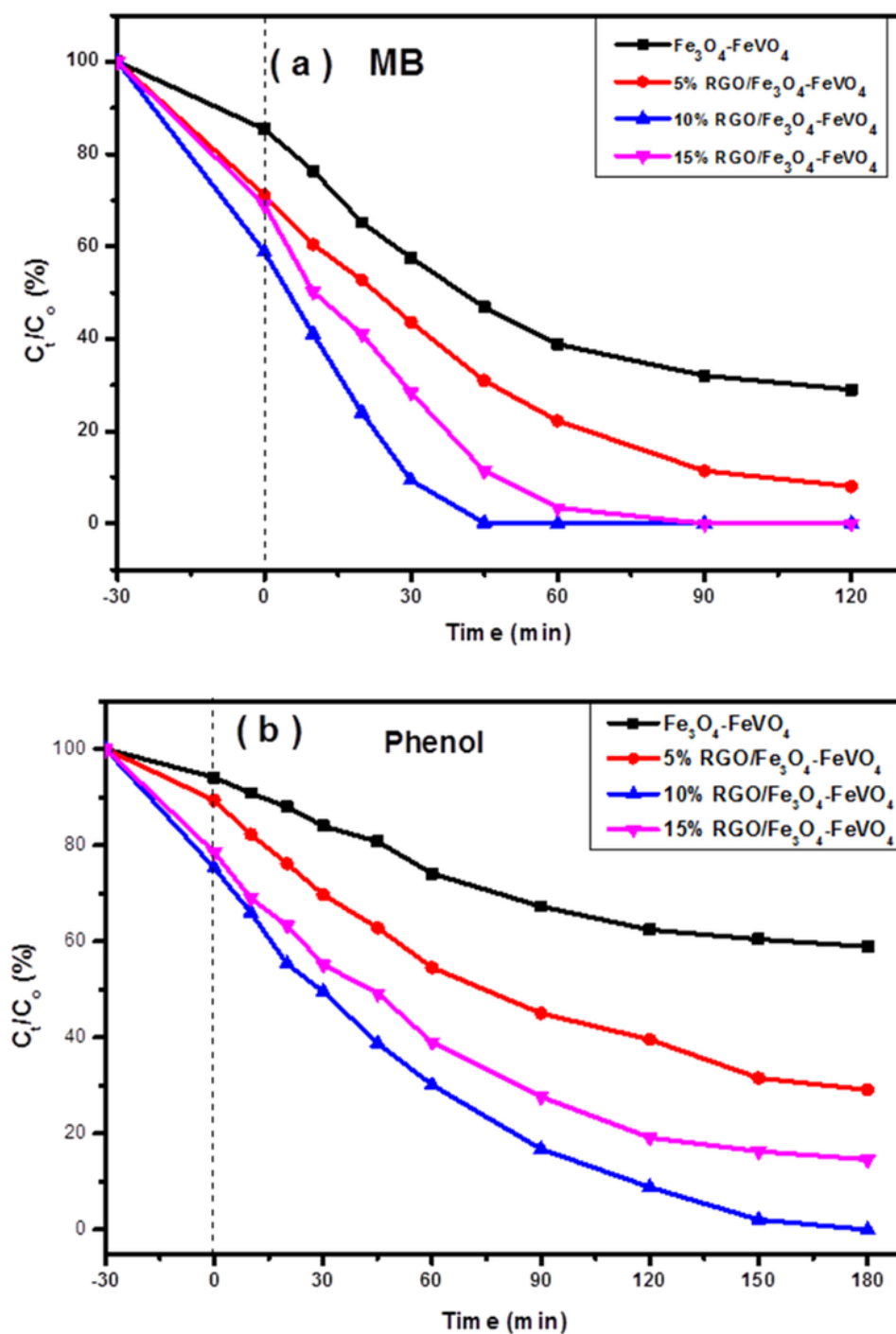


Figure 7

Photocatalytic degradation of (a) MB and (b) phenol over of $\text{Fe}_3\text{O}_4\text{-FeVO}_4$ and $x\text{RGO}/\text{Fe}_3\text{O}_4\text{-FeVO}_4$ nanocomposites vs. irradiation time

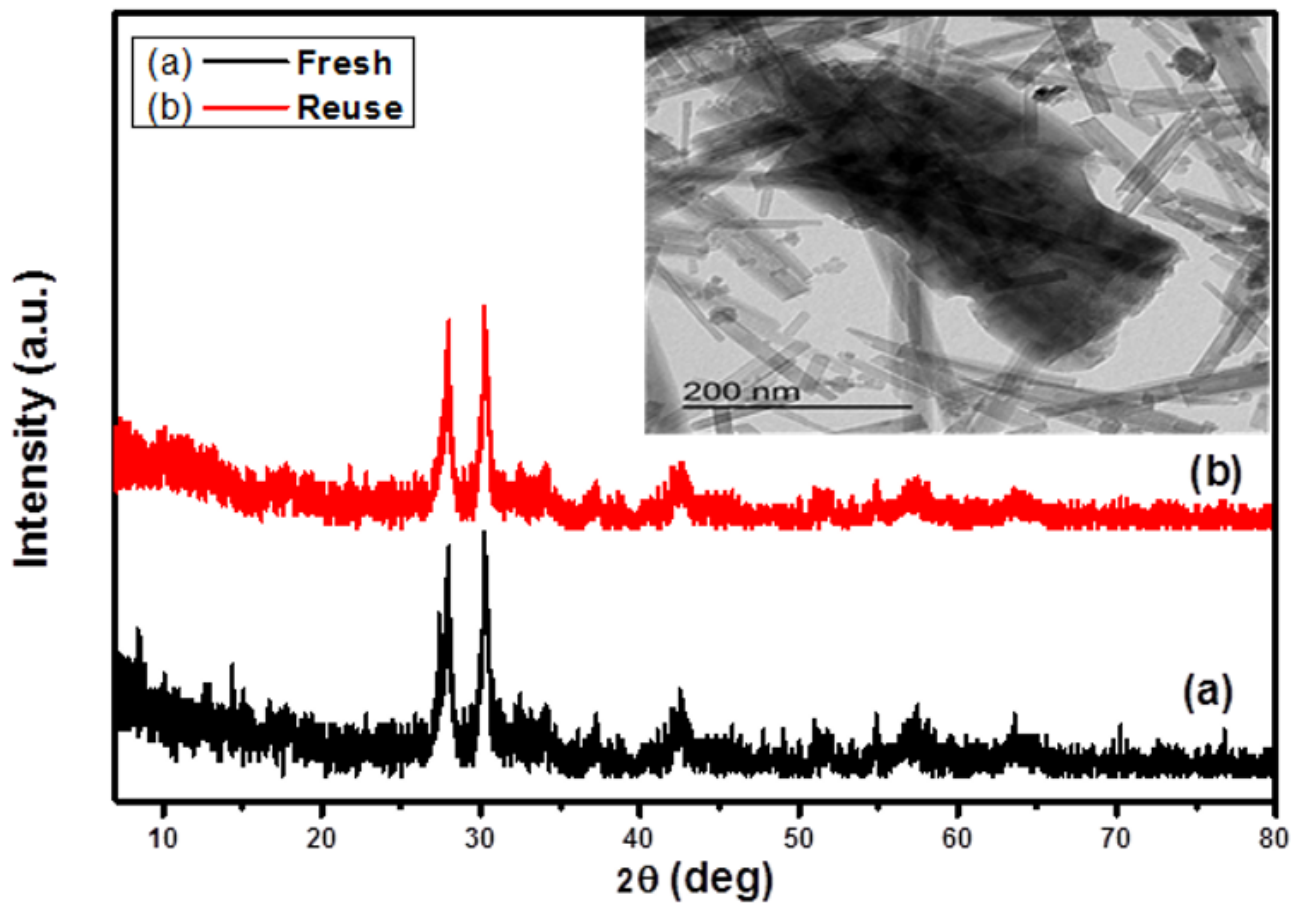


Figure 8

Effect of reuse on the structural properties of 10% rGO/FeVO₄ nanocomposites.

Supplementary Files

This is a list of supplementary files associated with this preprint. Click to download.

- [Supplementaryinformation.docx](#)